



Supplementary Materials for

An Inhibitor of Mutant IDH1 Delays Growth and Promotes Differentiation of Glioma Cells

Dan Rohle, Janeta Popovici-Muller, Nicolaos Palaskas, Sevin Turcan, Christian Grommes, Carl Campos, Jennifer Tsoi, Owen Clark, Barbara Oldrini, Evangelia Komisopoulou, Kaiko Kunii, Alicia Pedraza, Stefanie Schalm, Lee Silverman, Alexandra Miller, Fang Wang, Hua Yang, Yue Chen, Andrew Kernytsky, Marc K. Rosenblum, Wei Liu, Scott A. Biller, Shinsan M. Su, Cameron W. Brennan, Timothy A. Chan, Thomas G. Graeber, Katharine E. Yen,* Ingo K. Mellinghoff*

*Corresponding author.

E-mail: katharine.yen@agios.com (K.E.Y.); mellingi@mskcc.org (I.K.M.)

Published 4 April 2013 on *Science Express*

DOI: 10.1126/science.1236062

This PDF file includes:

Materials and Methods
Supplementary Text
Figs. S1 to S16
Tables S1 and S2
References

Materials and Methods

Determination of compound inhibition potency against the R132H. This assay was used for both the HTS and subsequent IC₅₀ determinations to map the SAR of evolved compounds. In the primary reaction, the reduction of α -KG acid to 2-HG is accompanied by a concomitant oxidation of NADPH to NADP. The amount of NADPH remaining at the end of the reaction time is measured in a secondary diaphorase/resazurin reaction in which the NADPH is consumed in a 1:1 molar ratio with the conversion of resazurin to the highly fluorescent resorufin. Uninhibited reactions exhibit a low fluorescence at the end of the assay, while reactions in which the consumption of NADPH by R132H IDH1 has been inhibited by a small molecule show a high fluorescence. The primary reaction was performed in a volume of 50 μ L 1X Buffer (150 mM NaCl, 20 mM Tris 7.5, 10 mM MgCl₂, 0.05% (w/v) bovine serum albumin), contained 2 nM R132H IDH1, 1 mM alpha-ketoglutarate, and 4 μ M NADPH, and was conducted for sixty minutes at 25°C. To perform the secondary reaction, 25 μ L of 1X buffer containing 36 μ g/mL diaphorase and 30 mM resazurin was added to the primary reaction and incubated for a further 10 minutes at 25°C. Florescence was read on a Spectramax platereader at Ex 544 Em 590. Recombinant protein was expressed and purified as described in (1). Compounds or compound dilutions were prepared in 100% DMSO concentration and diluted 1:100 into the final reaction. R132C IDH1 was assayed under similar conditions, with the exception that the 1X Buffer was 50 mM K₂HPO₄, pH 6.5; 40 mM NaHCO₃; 5 mM MgCl₂; 10% glycerol; 0.03% (w/v) bovine serum albumin.

Assay of the IDH1 wild-type enzyme reaction for determination of inhibitor potency to this non-targeted version of the enzyme. IDH1 wild-type enzyme was assayed in a modified version of the assay used for R132H IDH1. Since this enzyme converts NADP to NADPH stoichiometrically with the conversion of isocitrate to alpha-ketoglutarate, NADPH product can be continuously assayed by direct coupling to the diaphorase/resazurin system and reading resorufin production at Ex 544 Em 590. Assays were conducted in 50 μ L of 1X Buffer (150 mM NaCl; 20 mM Tris, pH 7.5; 10 mM MgCl₂; 0.05% (w/v) BSA; 2 mM B-ME) containing 50 μ M NADP, 70 μ M DL-isocitrate and 31.2 ng/mL IDH1wt enzyme. The direct coupling system was comprised of 20 μ g/ml diaphorase and 40 μ M resazurin.

Assay of the IDH2 R140Q and IDH2 R172K enzyme reaction for determination of inhibitor potency. Inhibitory potency against the IDH2 R140Q and IDH2 R172K enzymes was determined in an endpoint assay in which the amount of NADPH remaining at the end of the reaction was measured by the addition of a large excess of diaphorase and resazurin. IDH2 R140Q was diluted to 0.25 μ g/mL in 40 μ L 1X Assay Buffer (150 mM NaCl, 50 mM potassium phosphate pH 7.5, 10 mM MgCl₂, 10% glycerol, 2 mM B-ME, 0.03% BSA) and incubated for 16 hours at 25°C in the presence of 1 μ L of compound in DMSO. The reaction was started with the addition of 10 μ L of Substrate Mix (20 μ M NADPH, 8 μ M alpha-ketoglutarate, in 1X Assay Buffer) and incubated for 1 hour at 25°C. Then, remaining NADPH was measured by the addition of 25 μ L of Detection Mix (36 μ g/mL diaphorase, 18 μ M resazurin in 1X Assay Buffer), incubated for 5 minutes at 25°C, and read as described above. IDH2 R172K was assayed as for IDH2 R140Q with the following modifications: 1.25 μ g/mL of protein was used, the Substrate Mix contained 50 μ M NADPH and 6.4 μ M alpha-ketoglutarate, and the compound was incubated for 1 hour before starting the reaction.

Assay of the IDH2 wild-type enzyme reaction for determination of inhibitor potency to this non-targeted family member of the enzyme. Inhibitory potency of compounds against the IDH2 WT enzyme was determined in a coupled assay to diaphorase. In this assay, production of NADPH by IDH2 WT was linked to a concomitant reduction of resazurin to the highly fluorescent resorufin. Enzyme was diluted to 0.06 µg/mL in 40 µL 1X Assay Buffer (150 mM NaCl, 50 mM potassium phosphate pH 7, 10 mM MgCl₂, 10% glycerol, 2 mM B-ME, 0.03% BSA), to which 1 µL of compound was added in DMSO. The mixture was incubated for 1 hour at room temperature. The reaction was started with the addition of 10 µL of Substrate Mix (200 µM isocitrate, 175 µM NADP, 60 µg/ml diaphorase, 200 µM resazurin, in 1X Assay Buffer), and run for 30 minutes at room temperature. The reaction was halted with the addition of 25 µL of 6% SDS and read on a Spectramax Plate Reader at Ex544/Em590.

Glioma Cell Lines. TS603, TS676, and TS516 glioma cells were derived from glioma patients who underwent tumor resection at Memorial Sloan-Kettering Cancer Center (MSKCC). All human samples were collected after patients signed informed consent according to MSKCC IRB-guidelines. HT1080 cells were obtained from ATCC. Ink4a/Arf ^{-/-} neuroprogenitor cells (NPCs) were derived as previously described (2).

Generation of sublines with inducible IDH1 knockdown. TS603 cells and HT1080 cells were infected with lentiviral particles containing either pTRIPz empty vector (OpenBiosystems), pTRIPz IDH1 sh484 (targeting the CDS), or pTRIPz IDH1 sh1894 (targeting the 3'-UTR). To produce lentiviral particles, 293T cells were co-transfected with pTRIPz vectors, psPAX2 (Addgene #12260), and pMD2.G (Addgene #12259) and supernatant containing viral particles was collected at 36 and 72 hours.

Generation of lines with R132H-IDH1 overexpression. Immortalized Normal Human Astrocytes (NHAs) and Ink4a/Arf ^{-/-} neurospheres were infected with retroviral particles containing pQCXIH (Clontech #631516) or pQCXIH R132H-IDH1. NHAs were a kind gift from Russ Pieper (University of California, San Francisco.) Ink4a/ARF^{-/-} neuroprogenitor cells were isolated from the subventricular zone of mice 6 days after birth as previously described (2). To produce retroviral particles, GP2-293 cells were co-transfected with pQCXIH vectors and pVSV-G (Clontech #631512).

Soft Agar assays. Cells were seeded in triplicates at 150,000 cells/well in Neurocult media (Stem Cell Technologies) containing 0.4% Noble agar and growth factor supplements (20ng/mL EGF, 10ng/mL bFGF). Cells were plated between two layers of Neurocult media and growth factors containing 0.65% Nobel agar. Colonies were stained 4 weeks after plating with either crystal violet (0.005%) or thiazolyl blue tetrazolium bromide (Sigma, M5655) and quantified using imagine software (Oxford Optronix) and an image processing algorithm (Charm algorithm, Oxford Optronix).

In-vivo experiments. SCID mice were injected subcutaneously with 10⁶ glioma cells, which were suspended in 100 µL of a 50:50 mixture of growth media and Matrigel (BD #356237). Once tumors had reached a measurable size, mice were randomized into the indicated treatment groups. All experiments followed Institutional Animal Care and Use Committee (IACUC)-approved procedures.

Immunohistochemistry and Image Analysis. Paraffin-embedded tumor xenografts were sectioned at a thickness of 5 μm /slide. Antigen retrieval, immunohistochemical detection, and counter staining were performed using a Ventana Discovery Ultra autostainer (Ventana). Primary antibodies were diluted as indicated: cleaved caspase-3 (Cell Signaling, #9665) 1:1000, H3K9Me3 (Abcam, #8898) 1:300, and Ki67 (DAKO, #M7240) 1:100. To determine the percentage of immunohistochemical positive cells, we assessed the total number of positively stained nuclei \times 100/total number of nuclei on hematoxylin counterstaining. Three separate regions were analyzed for each tumor and captured with a camera (SPOT Imaging Solutions). Digitized images were segmented with segmentation techniques such as density and size thresholding to distinguish negative from positive objects using the image analysis software (ImageJ; NIH). The segmentation process resulted in the generation of binary images from which the number of stained objects and total numbers of nuclei was determined. Results were statistically analyzed using One-way ANOVA on GraphPad Prism 5.

In-vitro Differentiation Assays. Glass coverslips (Corning) were coated with PBS diluted laminin (Invitrogen, 23017-0015) for 2 hours, washed with PBS and then single cell dissociated cells were plated onto the coated coverslips at a density of 30,000/cm² and cells were allowed to attach overnight. The following day individual coverslips were placed into differentiating conditions (1% FBS with 1 μM retinoic acid) along with treatments for 4 or 7 days with the media being replenished on day 4. Cells were then fixed with 4% PFA for 30 minutes at room temperature, and permeabilized with a 0.05% triton-x solution. Primary antibodies were then applied; Nestin 1:200 (Millipore), GFAP 1:1000 (Dako), and DAPI followed by secondary antibodies with fluorescent tags (Invitrogen), and then mounted on slides. Digitized Images were obtained and segmentation techniques such as density and size thresholding was done on 3 fields of view from each slide with an average of 1500 cells/view using ImageJ software (NIH).

Chromatin Immunoprecipitation: TS603 cells were grown in medium containing either AGI-5198 (1.5 μM) or DMSO vehicle control. One week prior to harvest cells were transferred to differentiation medium (DMEM F12; 15mM HEPES; 0.06% glucose; B27 without vitamin A; N2; Insulin/transferrin; 1% FBS) containing freshly added retinoic acid (1 μM). ChIP of non-cross-linked cells was then carried out using established ChIP methods. 350 μg of lysate was immunoprecipitated-using anti-H3K9Me3 (ab8898, abcam), H3K27me3 (#9733S, Cell Signaling) or Rabbit Control IgG (ab46540, abcam). After washing, ChIP DNA was eluted from protein G beads and analyzed by RT-PCR using SYBR green (Applied Biosystems). Relative occupancy was calculated using the standard curve method and fold enrichment versus IgG. Enrichment in AGI-5198-treated cells was normalized to vehicle control. Means and standard deviation were calculated from 4 technical replicates.

RT-PCR. RNA was isolated from 20-30 mg of tumor tissue using the Qiagen RNeasy Plus protocol. RNA concentrations were then normalized and cDNA generated using the high-capacity cDNA reverse transcription protocol from Applied Biosciences (ABI catalog number 4368813). Q-PCR was on a 7900HT Fast Real Time PCR machine using a standard delta relative quantitation ($\Delta\Delta\text{RQ}$) QPCR protocol. Cycles length was 50C 2 minutes, 95C 10 minutes, then 40 cycles of 95C 15 seconds and 60C 1 minute. TaqMan (R) Gene Expression Assay: ATP1A2 (FAM): SMID: Hs00265131_m1, GFAP(FAM): SMID: Hs00909233_m1, APQ4(FAM): SMID: Hs00242342_m1, CNP(FAM): SMID: Hs00263981_m1, CSPG4(NG2)(FAM): SMID: Hs00426981_m1.

RNA and DNA Extraction. DNA and RNA was extracted from microdissected sections from TS603 xenografts that had been snap frozen in liquid nitrogen and stored at -80°C. Xenograft DNA was extracted with the Qiagen DNeasy Blood and Tissue Kit protocol, and xenograft RNA was

extracted using the Qiagen RNeasy Lipid Tissue protocol. In addition, DNA from TS603 cells treated with DMSO or 1.5uM AGI-5198 at passages 0, 2, 4, 15, and 20 was extracted using the Qiagen DNeasy Blood and Tissue Kit protocol.

Data Analysis. TS603 expression data was RMA normalized from the raw CEL files in Partek. Hierarchical clustering was performed on log transformed and normalized data. Analysis of variance was performed using Partek Genomic Suite and genes were filtered for p-value<0.05. Clustering was performed using Cluster 3.0 with average Pearson correlation as the similarity metric and visualized using Treeview. Functional analysis was performed using GSEA with the MolSigDB C2-pathways downloaded from the Broad Institute website (<http://www.broadinstitute.org/gsea/msigdb/collections.jsp>). The rank list was created by collapsing to max probe with signal to noise ratio as metric. One thousand permutations were employed to generate nominal p-values. Genes significantly (p-value <= 0.05) upregulated or downregulated in both AGI-5189 150 mg/kg and 450 mg/kg treatment groups with a fold change >=1.5 were selected. Enrichment analysis was performed using the Database for Annotation, Visualization and Integrated Discovery (DAVID) using all human genes as the background set and with Ingenuity IPA using Agilent Human Genome U133 Plus 2.0 probes as the background set. The methylation array beta value data was generated from intensity values using Genome Studio Software (Illumina) and imported into Partek. The β -values are given by $\beta = (\text{methylated probe intensity} / (\text{methylated probe intensity} + \text{unmethylated probe intensity}))$. TS603 xenograft delta beta values were calculated for all probes as $\text{delta} = \text{mean } \beta_{\text{treated}} - \text{mean } \beta_{\text{vehicle}}$. Corresponding intermediate grade glioma delta beta values were calculated as $\text{delta} = \text{mean } \beta_{\text{mutant}} - \text{mean } \beta_{\text{wildtype}}$.

CIMP Analysis in TS603 Cells. The previously published intermediate grade glioma (WHO Grade II/III) whole genome methylation beta values (3) were used to calculate mean beta values for each class and their frequency distribution was plotted alongside the vehicle-treated TS603 xenograft data without further normalization. Intermediate grade glioma (WHO Grade II/III) and high grade glioma (WHO Grade IV) methylation data was limited to only probes that corresponded to the transcription start sites (140,000 probes). The most variant probes were identified to create two unique sets of ~5000 probes that would define CIMP status. TS603 methylation data was then incorporated into either the LGG or the TCGA files, and the resulting datasets were analyzed with 2 dimensional hierarchical cluster on the un-standardized beta values using Pearson's dissimilarity as the similarity metric.

Integration of Methylation and Transcription Data. For our integrated analysis of DNA methylation and RNA expression changes, methylation data were logit transformed and gene expression data were log2 transformed after RMA normalization. We calculated p-values using a Student's t-test (two-sample equal variance). P-values were then negative log10 transformed for the purpose of visualization, assigned directionality based on IDH1 mutation (low grade glioma tumors) or treatment (mouse xenograft), and plotted on log-log scatter plots. Negative directionality corresponds to a decrease and positive directionality corresponds to an increase in transcription or methylation. Signed log10 p-values for transcription and methylation probes were matched by gene symbol, based on the annotations provided by respective platform manufacturers (Illumina and Affymetrix). Threshold lines on the log10 plots were drawn at -1.3 and 1.3 (p-value = 0.05). All RNA expression arrays and DNA methylation arrays were run at the Genomics Core Facility at Memorial Sloan-Kettering Cancer Center.

Beta and Delta Beta Values. β -values represent the ratio of methylated/(methylated + unmethylated) DNA and are reported for ~ 485,000 probes in the Infinium Human Methylation450 Arrays. Figure 4 B shows the distribution of β -values in vehicle versus AGI-5198 treated TS603 xenograft tumors. For the prolonged in vitro exposure of TS603 cells (Fig. S16), delta beta values were calculated from biological duplicates as $\text{delta} = \text{mean } \beta_{\text{treated}} - \text{mean } \beta_{\text{vehicle}}$ for each of the four passage points. Delta beta values greater than 0.2 or less than -0.2 were included in the overlap analysis.

Hierarchical Clustering. For analysis of gene expression patterns from AGI-5198-treated TS603 glioma xenografts, clustering was performed on log transformed and normalized data. Analysis of variance was performed using Partek Genomic Suite and genes were filtered for p -value < 0.05 . Clustering was performed using Cluster 3.0 with average Pearson correlation as the similarity metric and visualized using Treeview. Probes were filtered using an ANOVA p -value threshold of 0.05 between the three treatment groups ($n = 6492$ probes).

Supplementary Text

Changes in DNA methylation during prolonged in-vitro culture with mIDH1 inhibitor. Treatment of leukemia cells with the DNA methyltransferase inhibitor decitabine (DAC) has been reported to result in DNA hypomethylation (i.e., a left-shift in the β -value distribution) within a timeframe of days (4). This is in contrast to our observations following acute inhibition of mutant IDH1 in glioma cells. Active DNA demethylation involves multiple steps after the initial hydroxylation of 5-methylcytosine by TET proteins (5) and may follow slower kinetics than passive demethylation occurring when maintenance DNA methylation is blocked. We therefore examined the effects of AGI-5198 on genome-wide DNA methylation during prolonged drug exposure in-vitro. We cultured TS603 glioma cells continuously in the presence of 1.5 μ M AGI-5198 or vehicle, collected DNA samples at multiple passage numbers (# 2, #4, #15, #20), hybridized the DNA to methylation arrays, and determined the difference in DNA methylation between AGI-5198 and vehicle treated cells (expressed as a delta- β -value for each probe). Independent biological replicates were collected for each condition. At early passage numbers (passage # 2 and 4), we noted a narrow distribution of delta β -values indicating no significant differences in DNA methylation between vehicle and AGI-5198 treated samples. The number of probes with a decrease in delta β -value (demethylation) of 0.2 or greater increased markedly between the two early passages ($n=3$ and $n=7$ probes, respectively) and the late passages ($n=8012$ and $n=6746$ probes, respectively). The majority of probes ($5935/8012 = 74.1\%$) with a decrease in delta β -value of 0.2 or greater at passage 15 also showed a similar or greater decrease in DNA methylation at passage 20 (Fig.S16) whereas we observed minimal overlap (1 probe) between the two early passages. While these data point to an active role of the mutant IDH1 enzyme in epigenetic remodeling, changes in DNA methylation in response to inhibition of the mutant enzyme were limited to a small fraction of the genome ($< 2\%$) and followed kinetics that are unlikely to drive gene expression changes within the short timeframe of our in-vivo xenograft experiments.

Gene expression programs associated with in-vivo growth inhibition by mutant IDH1 inhibitor. To identify pathways that are associated with the growth-inhibitory effects of AGI-5198, we ran Affymetrix RNA expression arrays for all TS603 xenograft tumors in the AGI-5198 dose-response experiment for which we were able to isolate RNA and DNA of sufficient quality and quantity (23/30 total tumors). 41 probes showed a statistically significant ($p<0.05$) change in RNA expression (≥ 1.5 -fold) in both AGI-5198 treated cohorts (i.e., 150 mg/kg and 450 mg/kg groups)(Table S2). Functional annotation algorithms (Ingenuity® Systems, www.ingenuity.com)

assign many of these genes to Cardiovascular System Development and Function (PER1, CTGF, GADD45A, LEPR, PIK3R1, ACTA2, PECAM1) and Tissue Morphology (PER1, CHRNA1, CALCRL, CTGF, LEPR, PIK3R1, ACTA2, PTGDS, TSC22D3, SERPINE2, SLITRK6, GADD45A, PROS1, ST8SIA2, PECAM1).

Integrated analysis of DNA methylation and RNA expression data. An integrated analysis of the DNA methylation data and RNA expression data showed that, in contrast to human gliomas where anti-correlated DNA methylation and gene expression changes are readily appreciated in a comparison between IDH-mutant and IDH wildtype tumors (Fig.S15A), much less change – and no correlation – is seen in a comparison of AGI-5198 and vehicle treated R132H-*IDH1* mutant glioma xenografts (Fig.S15B/C).

References

1. L. Dang *et al.*, Cancer-associated IDH1 mutations produce 2-hydroxyglutarate. *Nature* **462**, 739 (2009). [doi:10.1038/nature08617](https://doi.org/10.1038/nature08617)
2. C. Lu *et al.*, IDH mutation impairs histone demethylation and results in a block to cell differentiation. *Nature* **483**, 474 (2012). [doi:10.1038/nature10860](https://doi.org/10.1038/nature10860)
3. S. Turcan *et al.*, IDH1 mutation is sufficient to establish the glioma hypermethylator phenotype. *Nature* **483**, 479 (2012). [doi:10.1038/nature10866](https://doi.org/10.1038/nature10866)
4. H.-C. Tsai *et al.*, Transient low doses of DNA-demethylating agents exert durable antitumor effects on hematological and epithelial tumor cells. *Cancer Cell* **21**, 430 (2012). [doi:10.1016/j.ccr.2011.12.029](https://doi.org/10.1016/j.ccr.2011.12.029)
5. J. S. You, P. A. Jones, Cancer genetics and epigenetics: Two sides of the same coin? *Cancer Cell* **22**, 9 (2012). [doi:10.1016/j.ccr.2012.06.008](https://doi.org/10.1016/j.ccr.2012.06.008)

Supplementary Figures

Fig. S1.

Assay for determination of compound inhibition potency against the *R132H-IDH1* enzyme.

A Diaphorase/Resazurin coupled system reaction was used for both the High-Throughput Screen and subsequent IC50 determinations to map the SAR of compounds (see Methods Section).

Fig. S2

Pharmacokinetic in-vivo profile of AGI-5198 in TS603 glioma xenografts.

(A) Dosing schedule for pharmacokinetic analysis of AGI-5198 in TS603 xenograft bearing mice.

(B) Concentration of AGI-5198 measured in plasma and tumor samples.

Fig. S3

Treatment with AGI-5198 does not result in loss of body weight.

Shown are the body weight of *SCID* mice treated daily with AGI-5198 (450mg/kg daily by gavage; n=20 per group).

Fig. S4

mIDH1 inhibitor reduces proliferation of *R132H-IDH1* mutant glioma cells in mice.

Shown is immunohistochemistry (IHC) of TS603 xenografts treated with vehicle (top) or AGI-5198 (bottom). TS603 glioma xenografts show reduced staining for Ki-67 (left panel), but no difference in staining for cleaved caspase-3 (right panel). Tumors were harvested after 16 days of treatment with AGI-5198. Scale bar = 100 μ M.

Fig. S5

IDH1-knockdown impairs growth of *R132H-IDH1* mutant glioma cells in soft-agar.

Shown are the number of colonies of *R132H-IDH1* glioma cells (TS603) engineered to express two different doxycycline-inducible IDH1-shRNAs and grown in soft agar in absence or presence of doxycycline (DOX) (* p < 0.05).

Fig. S6

Doxycycline does not impair the in-vivo growth of *R132H-IDH1* glioma cells (TS603).

Shown are tumor volumes of TS603 cells engineered to express the empty shRNA vector and treated with doxycycline. Doxycycline-containing chow was started after subcutaneous xenograft tumors were established. n = 15 mice per cohort.

Fig. S7

Depletion of mIDH1 protein and intratumoral *R*-2HG in TS603-IDH1-shRNA xenograft tumors from doxycycline-treated mice.

The left panel shows IHC with an R132H-IDH1 specific antibody. The right panel shows intratumoral *R*-2HG concentrations. Mice were treated with doxycycline, vehicle, or AGI-5198 as indicated in the text. Scale bar =100 μ M. n=15 mice per cohort.

Fig. S8

IDH1 knockdown impairs growth of R132C-IDH1 mutant HT1080 fibrosarcoma cells.

(A) Western blot of HT1080 cells that were engineered to express empty vector or two doxycycline-inducible IDH1 shRNAs and treated with 2.5 μ g/mL doxycycline (DOX) or vehicle for 4 days. (B) Doxycycline-induced IDH1 knockdown impairs colony formation of HT1080 cells in soft agar (* p < 0.05). (C) HT1080 xenografts that harbor the inducible IDH1 shRNA show impaired growth when mice are treated with doxycycline (* p < 0.05). n = 11 mice per cohort. Doxycycline was started after subcutaneous tumors were established.

Fig. S9

R132H-IDH1 mutant TS603 glioma cells and *IDH1/2*-mutant gliomas show an increased number of hypermethylated gene loci using Illumina Infinium Human Methylation450 Arrays.

Shown is a comparison of genome wide DNA methylation (β value distribution) of IDH1- mutant TS603 xenografts (n=6), IDH1/2- mutant human gliomas (n=49), and IDH1/2-wildtype gliomas (n=31). Note the increased number of highly-methylated probes (β values > 0.7) in IDH1/2-mutant gliomas and IDH1- mutant TS603 glioma xenografts (compared to IDH1/2-wildtype gliomas).

Fig. S10

R132H-IDH1 mutant TS603 glioma cells are G-CIMP positive.

IDH1- mutant TS603 glioma cells cluster with *IDH1/2*-mutant glioblastomas (WHO grade IV) (A) and *IDH1/2*-mutant intermediate grade gliomas (WHO Grade II/III) (B). Unsupervised two-dimensional hierarchical clustering was performed using the top ~5000 most variant (β value) transcription start site (TSS) methylation probes (see Methods Section).

Fig. S11

AGI-5198 (450 mg/kg) reduces H3K9m3 levels in IDH1 mutant glioma cells.

Shown are representative images of R132H-*IDH1* mutant TS603 glioma xenografts treated with either vehicle (top left) or 450 mg/kg AGI-5198 (bottom left). The top right and bottom right panels show a negative (external granule cell layer of p7 murine cerebellum) and a positive (murine myocardium, E16.5) staining control. Scale bar = 50 μ M.

Fig. S12

AGI-5198 does not affect H3K9M3 methylation in IDH1-wildtype cells.

(A) Quantification of H3K9 trimethylation in IDH1-wildtype glioma xenografts (TS516) treated for two weeks with vehicle, 150 mg/kg AGI-5198, or 450 mg/kg AGI-5198. (B) Western blot of NHAs engineered to express empty vector (pQCXIH) or R132H-IDH1 (pQCXIH) and treated with AGI-5198 (1.5 μ M) for the indicated time (in days). NHAs were a kind gift from Russ Pieper (University of California, San Francisco.)

Fig. S13

AGI-5198 impairs tumor cell proliferation in R132H-IDH1 glioma xenografts.

Shown are representative Ki-67 IHC images (left) and image quantification (% positive cells)(right) from mice treated with for two weeks with vehicle, 150 mg/kg AGI-5198, or 450 mg/kg AGI-5198 (* $p < 0.05$). White scale bars represent 200 μ M. $n=15$ mice per cohort.

Fig. S14

Hierarchical clustering of genome wide RNA expression from vehicle and AGI-5198-treated TS603 glioma xenografts.

Clustering was performed on log transformed and normalized data (see Methods Section).

Fig. S15

AGI-5198-induced changes in RNA expression (x-axis) correlate poorly with changes in DNA methylation (y-axis) in R132H-*IDH1* glioma xenografts.

The relationship between *IDH1*-mutation associated differences in RNA expression and DNA methylation in human low grade gliomas is shown in (A) as a point of reference. Signed log₁₀ p-values express the statistical significance of the difference. Threshold lines are drawn to represent statistical significance at $p\text{-value}=0.05$ ($\log_{10}(0.05) = 1.3$). Directionality (sign) is assigned based on increasing (positive) or decreasing (negative) methylation (y-axis) or RNA expression (x-axis)(see Methods Section). Green data points represent probes with significant decrease in methylation and increase in gene expression (methylation signed log₁₀ p-value <-1.3 , gene expression signed log₁₀ p-value >1.3). Red data points represent probes with a significant increase in methylation and decrease in gene expression (methylation signed log₁₀ p-value >1.3 , gene expression signed log₁₀ p-value <-1.3). While anti-correlated DNA methylation and RNA expression changes are obvious in the comparison of IDH-mutant versus IDH-wildtype human

gliomas (A), much less change – and no correlation – is seen in response to mIDH1-inhibitor treatment of the xenografts tumors (B: 150 mg/kg, C: 450 mg/kg).

Fig. S16

Progressive changes in DNA methylation during continued in-vitro exposure of R132H-*IDH1* TS603 cells to AGI-5198.

Shown is the number of probes on the Illumina Infinium Human Methylation 450 Arrays that show a decrease in DNA-methylation ($\Delta \beta < -0.2$) between vehicle and AGI-5198 treated cells at each indicated passage number. Replicate arrays were run for all conditions. Note the increasing number of probes that show a consistent change in DNA methylation (Venn Diagram) between the two early passages (passage # 2 and # 4, top) versus two late passages (passage # 15 and 20, bottom).

Table S1.

List of genes that are upregulated or downregulated in TS603 xenografts in response to AGI-5198 treatment (compared to vehicle).

Direction	Rank	Fold Change	Probeset ID	Gene Symbol	Gene Title	p-value
UP	1	6.8	209904_at	TNNC1	troponin C type 1 (slow)	0.000
UP	2	5.9	202404_s_at	COL1A2	collagen, type I, alpha 2	0.001
UP	3	5.7	225275_at	EDIL3	EGF-like repeats and discoidin I-like domains 3	0.009
UP	4	4.3	239430_at	IGFL1	insulin growth factor-like family member 1	0.001
UP	5	4.0	213764_s_at	MFAP5	microfibrillar associated protein 5	0.002
UP	6	3.9	211748_x_at	PTGDS	prostaglandin D2 synthase 21kDa (brain)	0.001
UP	7	3.8	212187_x_at	PTGDS	prostaglandin D2 synthase 21kDa (brain)	0.001
UP	8	3.7	229218_at	COL1A2	Collagen, type I, alpha 2	0.001
UP	9	3.6	202403_s_at	COL1A2	collagen, type I, alpha 2	0.004
UP	10	3.3	201163_s_at	IGFBP7	insulin-like growth factor binding protein 7	0.009
UP	11	3.3	228854_at	ZBTB16	zinc finger and BTB domain containing 16	0.000
UP	12	3.3	218002_s_at	CXCL14	chemokine (C-X-C motif) ligand 14	0.003
UP	13	3.1	222484_s_at	CXCL14	chemokine (C-X-C motif) ligand 14	0.002
UP	14	2.9	201058_s_at	MYL9	myosin, light polypeptide 9, regulatory	0.003
UP	15	2.8	211663_x_at	PTGDS	prostaglandin D2 synthase 21kDa (brain)	0.002
UP	16	2.7	213765_at	MFAP5	microfibrillar associated protein 5	0.001
UP	17	2.5	202237_at	NNMT	nicotinamide N-methyltransferase	0.004
UP	18	2.4	206029_at	ANKRD1	ankyrin repeat domain 1 (cardiac muscle)	0.003
UP	19	2.3	209047_at	AQP1	aquaporin 1 (Colton blood group)	0.049
UP	20	2.2	200974_at	ACTA2	actin, alpha 2, smooth muscle, aorta	0.035
UP	21	2.2	203186_s_at	S100A4	S100 calcium binding protein A4 (calcium protein, calvasculin, metastasin, murine placental homolog)	0.001
UP	22	2.2	209616_s_at	CES1	carboxylesterase 1 (monocyte/macrophage serine esterase 1)	0.029
UP	23	2.1	202238_s_at	NNMT	nicotinamide N-methyltransferase	0.013
UP	24	2.1	229978_at	LOC440338	hypothetical gene supported by AJ002784	0.005
UP	25	2.1	226228_at	AQP4	aquaporin 4	0.016
UP	26	2.1	230425_at	EPHB1	EPH receptor B1	0.042
UP	27	2.0	201150_s_at	TIMP3	TIMP metalloproteinase inhibitor 3 (Sorsby fundus dystrophy, pseudoinflammatory)	0.009
UP	28	2.0	209101_at	CTGF	connective tissue growth factor	0.001

UP	29	2.0	223631_s_at	C19ORF33	chromosome 19 open reading frame 33	0.026
UP	30	2.0	203296_s_at	ATP1A2	ATPase, Na ⁺ /K ⁺ transporting, alpha 2 (+) polypeptide	0.045
UP	31	2.0	203878_s_at	MMP11	matrix metalloproteinase 11 (stromelysin 3)	0.011
DOWN	1	2.4	1552714_at	CREG2	cellular repressor of E1A-stimulated genes 2	0.003
DOWN	2	2.3	204338_s_at	RGS4	regulator of G-protein signalling 4	0.017
DOWN	3	2.2	231489_x_at	---	Transcribed locus, weakly similar to NP_694983.1 hypothetical protein FLJ25952 [Homo sapiens]	0.011
DOWN	4	2.1	236297_at	---	CDNA FLJ45742 fis, clone KIDNE2016327	0.033
DOWN	5	2.1	228708_at	RAB27B	RAB27B, member RAS oncogene family	0.043
DOWN	6	2.0	206214_at	PLA2G7	phospholipase A2, group VII (platelet-activating factor acetylhydrolase, plasma) /// phospholipase A2, group VII (platelet-activating factor acetylhydrolase, plasma)	0.011
DOWN	7	2.0	235236_at	DOCK2	Dedicator of cytokinesis 2	0.022

Table S2.

List of genes that are upregulated or downregulated (compared to vehicle) in TS603 glioma xenografts treated with both doses of AGI-5198 (150 mg/kg and 450 mg/kg).

Direction	Probeset ID	Gene Symbol	Gene Title	150 mg/kg p-value	150 mg/kg fold change	450 mg/kg p-value	450 mg/kg fold change
UP	212187_x_at	PTGDS	prostaglandin D2 synthase 21kDa (brain)	0.005	3.389	0.001	3.273
UP	211748_x_at	PTGDS	prostaglandin D2 synthase 21kDa (brain)	0.005	3.319	0.001	3.125
UP	206633_at	CHRNA1	cholinergic receptor, nicotinic, alpha 1 (muscle)	0.019	3.648	0.008	2.943
UP	211663_x_at	PTGDS	prostaglandin D2 synthase 21kDa (brain)	0.006	3.039	0.001	2.791
UP	1556138_a_at	COL5A1	Collagen, type V, alpha 1	0.010	2.268	0.000	2.422
UP	213056_at	FRMD4B	FERM domain containing 4B	0.003	2.207	0.010	2.074
UP	239537_at	ST8SIA2	ST8 alpha-N-acetylneuraminidase alpha-2,8-sialyltransferase 2	0.019	1.990	0.021	2.015
UP	228335_at	CLDN11	claudin 11	0.013	1.912	0.023	1.906
UP	203810_at	DNAJB4	DnaJ (Hsp40) homolog, subfamily B, member 4	0.027	1.616	0.003	1.862
UP	208763_s_at	TSC22D3	TSC22 domain family, member 3	0.000	2.172	0.014	1.852
UP	225768_at	NR1D2	nuclear receptor subfamily 1, group D, member 2	0.001	1.648	0.000	1.845
UP	209833_at	CRADD	CASP2 and RIPK1 domain containing adaptor with death domain	0.002	1.604	0.001	1.841
UP	1552703_s_at	CARD16 /// CASP1	caspase recruitment domain family, member 16 /// caspase 1, apoptosis-related cysteine	0.020	1.958	0.041	1.785
UP	234996_at	CALCRL	calcitonin receptor-like	0.029	1.539	0.036	1.708
UP	221307_at	KCNIP1	Kv channel interacting protein 1	0.033	1.455	0.003	1.687
UP	209101_at	CTGF	connective tissue growth factor	0.002	1.892	0.011	1.675
UP	201136_at	PLP2	proteolipid protein 2 (colonic epithelium-enriched)	0.001	1.758	0.016	1.654
UP	203543_s_at	KLF9	Kruppel-like factor 9	0.006	1.562	0.000	1.652
UP	202411_at	IFI27	interferon, alpha-inducible protein 27	0.049	1.465	0.023	1.652

UP	226582_at	LOC400043	uncharacterized LOC400043	0.016	1.616	0.019	1.642
UP	222717_at	SDPR	serum deprivation response	0.026	1.647	0.022	1.633
UP	228854_at	ZBTB16	zinc finger and BTB domain containing 16	0.022	1.717	0.039	1.618
UP	239638_at	---	---	0.000	1.751	0.002	1.593
UP	212239_at	PIK3R1	phosphoinositide-3-kinase, regulatory subunit 1 (alpha)	0.001	1.832	0.033	1.572
UP	203725_at	GADD45A	growth arrest and DNA-damage-inducible, alpha	0.002	1.512	0.000	1.566
UP	209894_at	LEPR	leptin receptor	0.002	1.916	0.038	1.560
UP	207808_s_at	PROS1	protein S (alpha)	0.007	1.516	0.012	1.557
UP	200974_at	ACTA2	actin, alpha 2, smooth muscle, aorta	0.008	1.633	0.024	1.534
UP	202861_at	PER1	period homolog 1 (Drosophila)	0.000	1.787	0.017	1.530
UP	208982_at	PECAM1	platelet/endothelial cell adhesion molecule 1	0.002	1.741	0.004	1.528
UP	208025_s_at	HMGA2	high mobility group AT-hook 2	0.040	1.458	0.043	1.520
UP	230876_at	ZNF883	zinc finger protein 883	0.001	1.861	0.034	1.512
UP	231270_at	CA13 /// LOC100507258	carbonic anhydrase XIII /// uncharacterized LOC100507258	0.020	1.556	0.039	1.498
DOWN	201295_s_at	WSB1	WD repeat and SOCS box containing 1	0.019	-1.539	0.006	-1.659
DOWN	235976_at	SLITRK6	SLIT and NTRK-like family, member 6	0.014	-1.706	0.004	-1.775
DOWN	212190_at	SERPINE2	serpin peptidase inhibitor, clade E (nexin, plasminogen activator inhibitor type 1), member 2	0.011	-1.699	0.003	-1.806
DOWN	206973_at	PPFIA2	protein tyrosine phosphatase, receptor type, family 1 polypeptide (PTPRF), interacting protein	0.014	-1.507	0.002	-1.823
DOWN	212909_at	LYPD1	LY6/PLAUR domain containing 1	0.008	-1.496	0.000	-1.853
DOWN	232176_at	SLITRK6	SLIT and NTRK-like family, member 6	0.044	-1.619	0.011	-1.857
DOWN	228186_s_at	RSPO3	R-spondin 3	0.034	-1.915	0.035	-2.009
DOWN	232481_s_at	SLITRK6	SLIT and NTRK-like family, member 6	0.007	-1.901	0.001	-2.081

Fig.S1

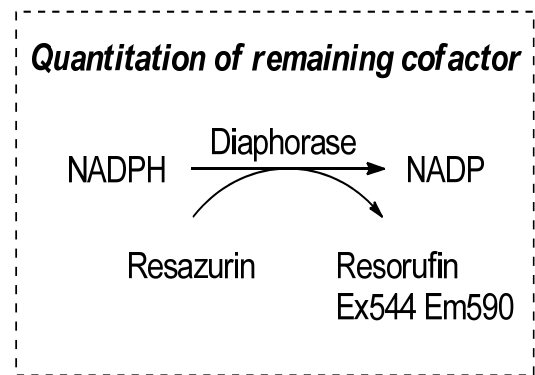
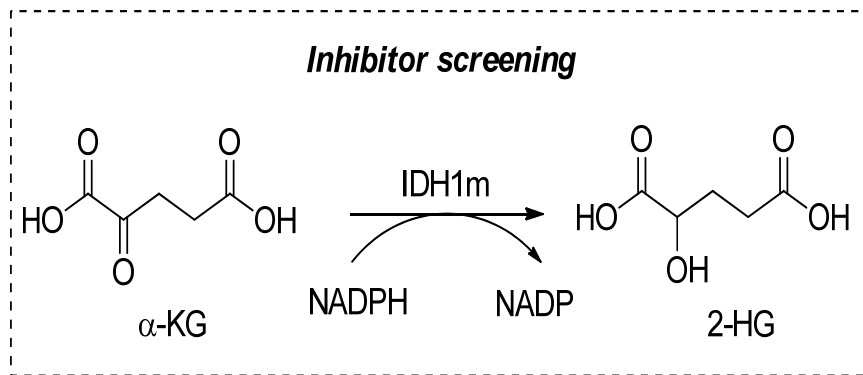
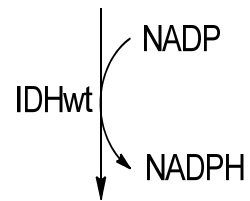
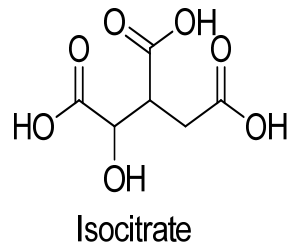


Fig.S2

A

Dose (mpk)	# of time point	# of Dose	Comments	Time points (hr) post last dose
50	5	3	BID 12 hr interval	1, 3, 8, 12, 24
150	5	3	BID 12 hr interval	1, 3, 8, 12, 24
Vehicle	8	3	BID 12 hr interval	0

B

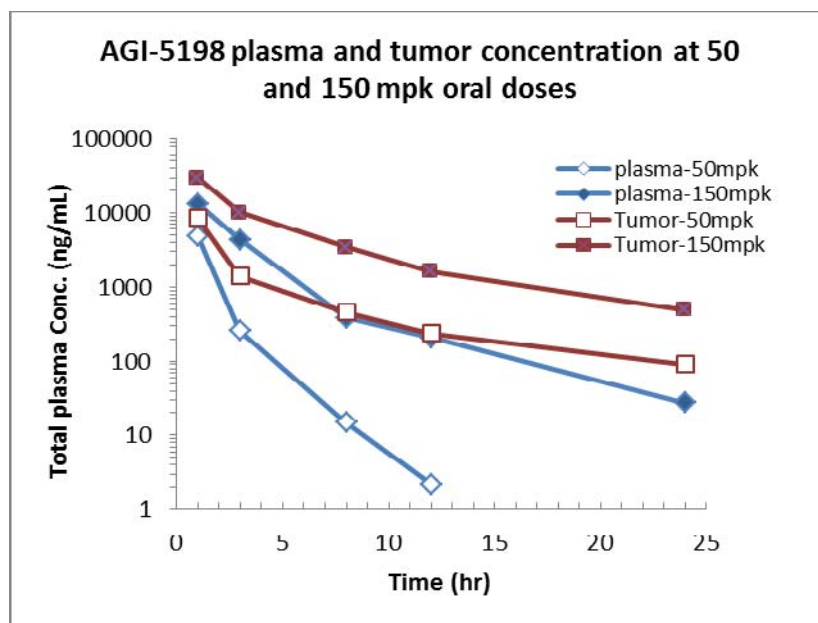


Fig.S3

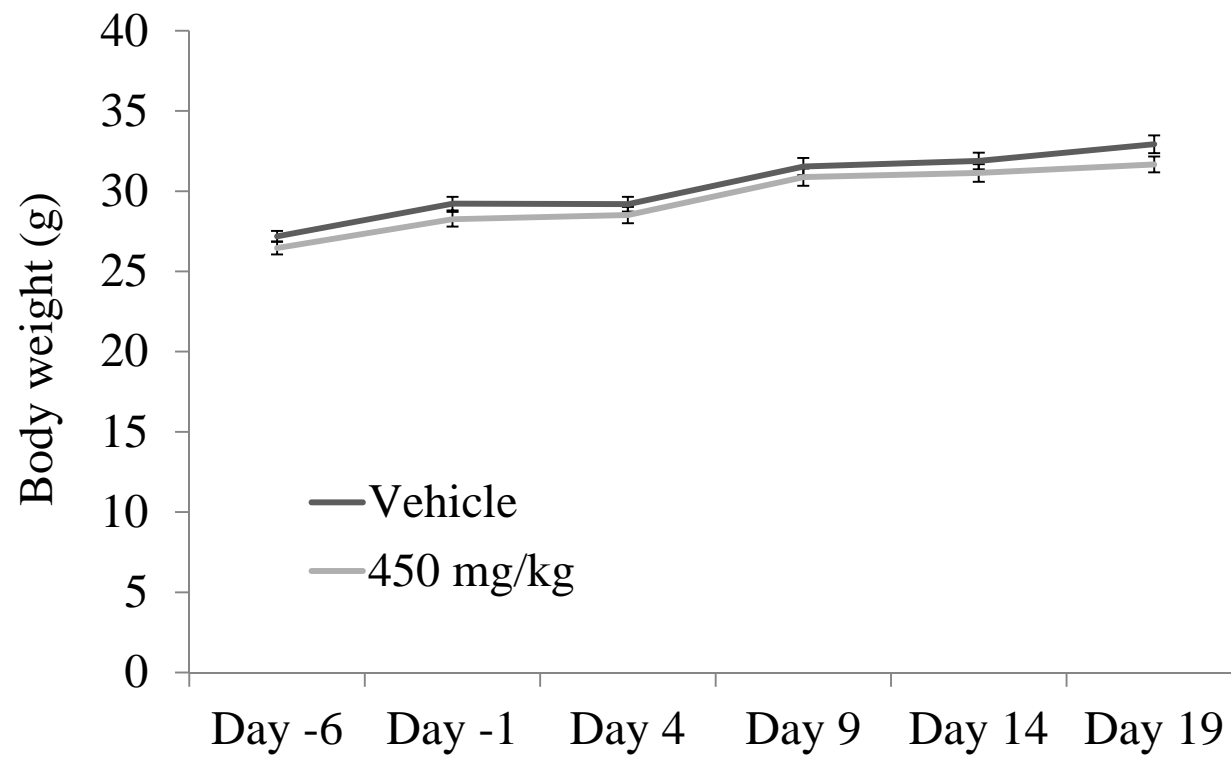


Fig.S4

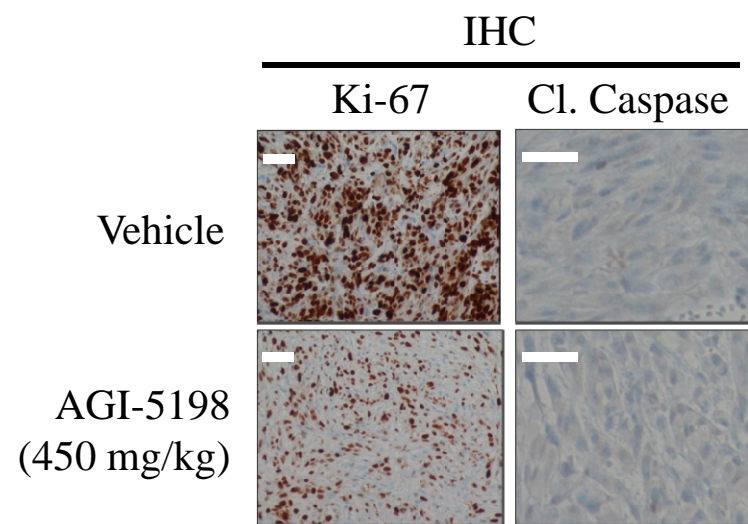


Fig.S5

R132H-IDH1
(TS603 glioma)

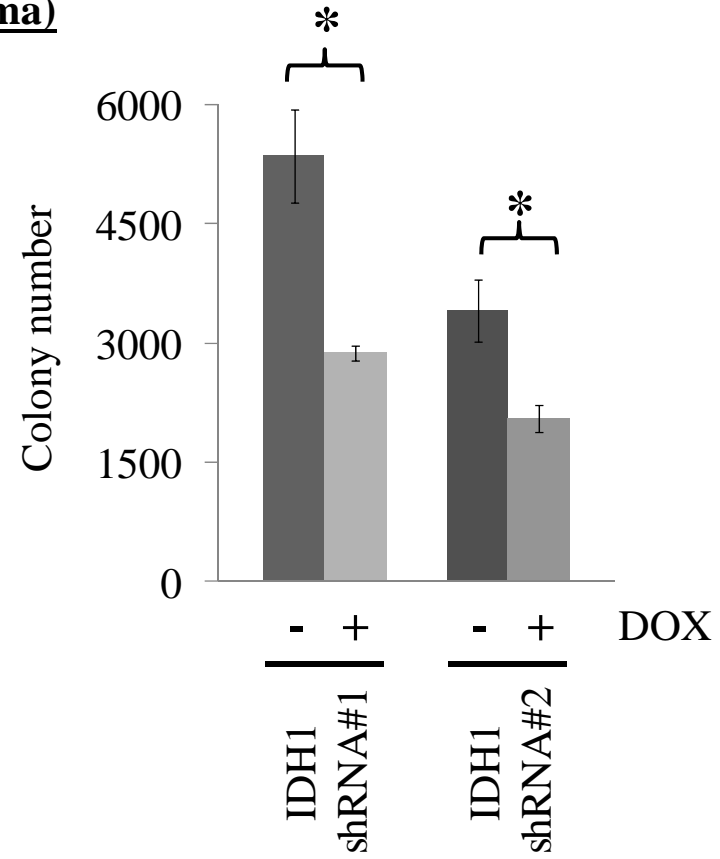


Fig.S6

R132H-IDH1
(TS603 glioma)

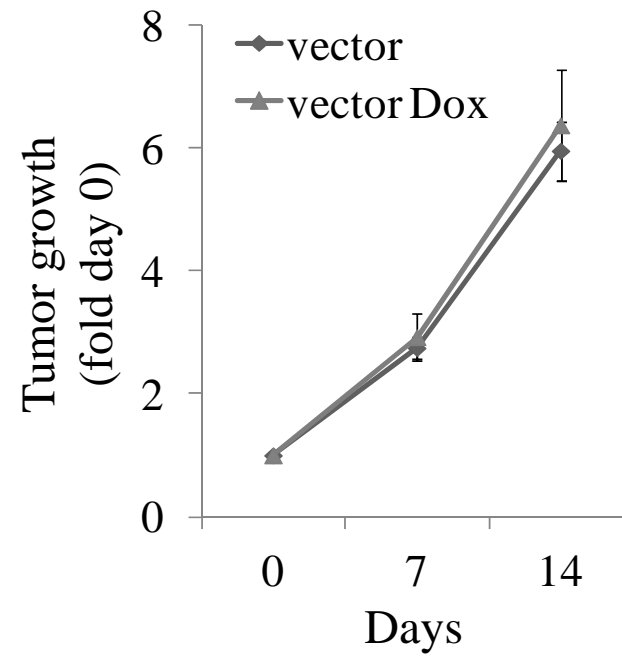


Fig.S7

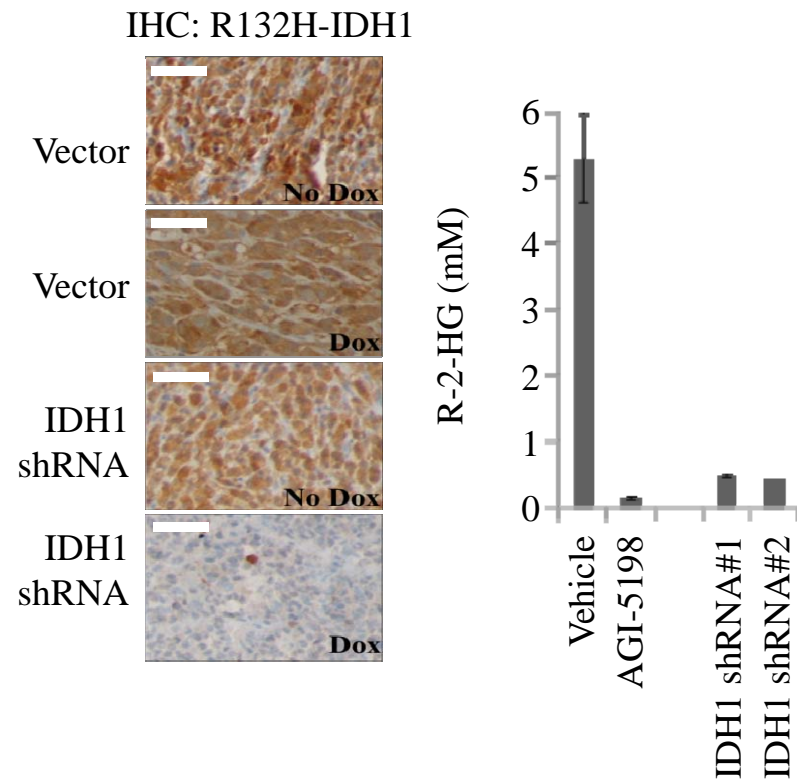
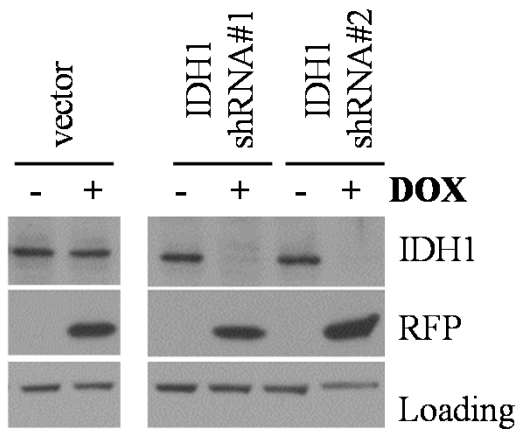
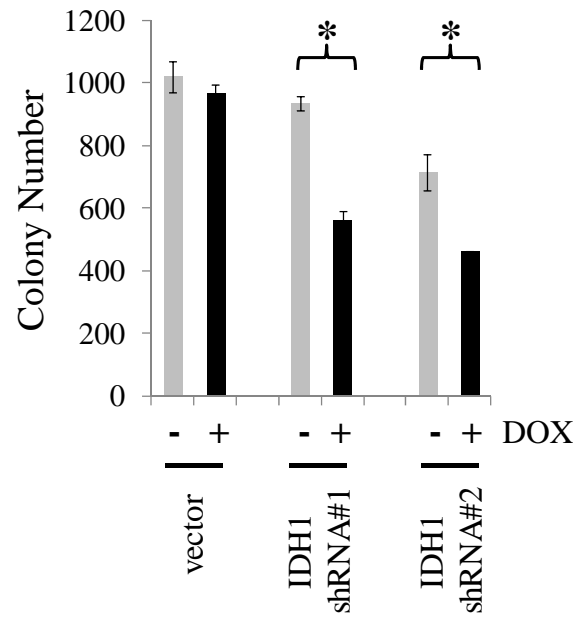


Fig.S8

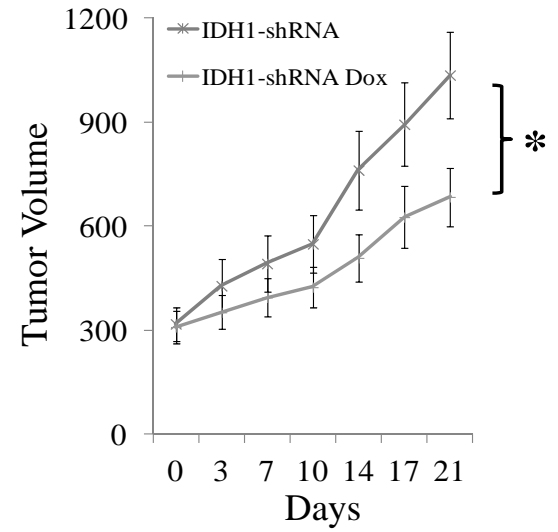
A



B



C



HT1080 Fibrosarcoma
R132C-IDH1

Fig.S9

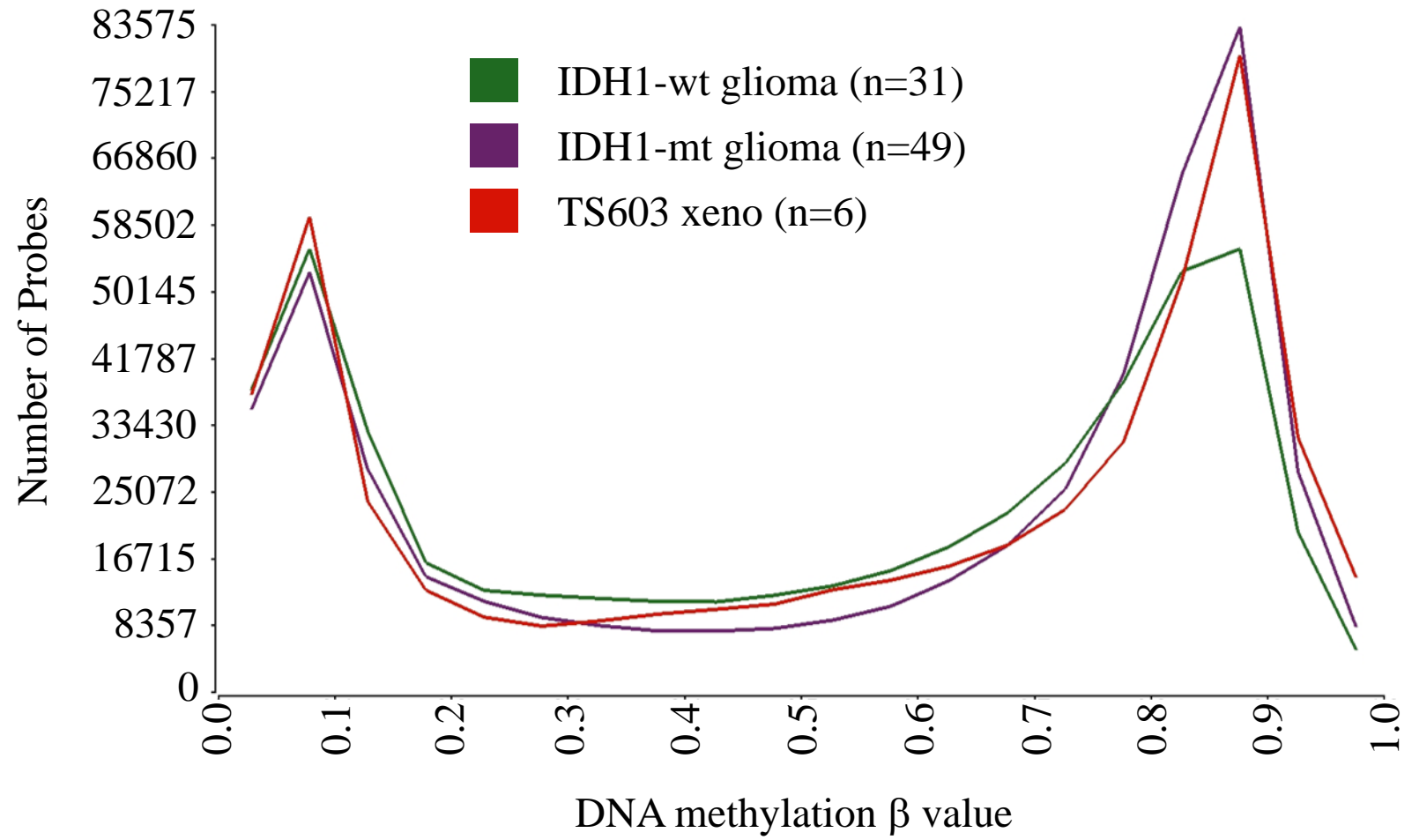
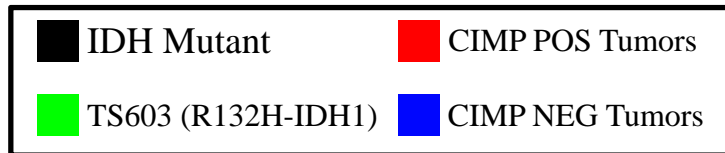
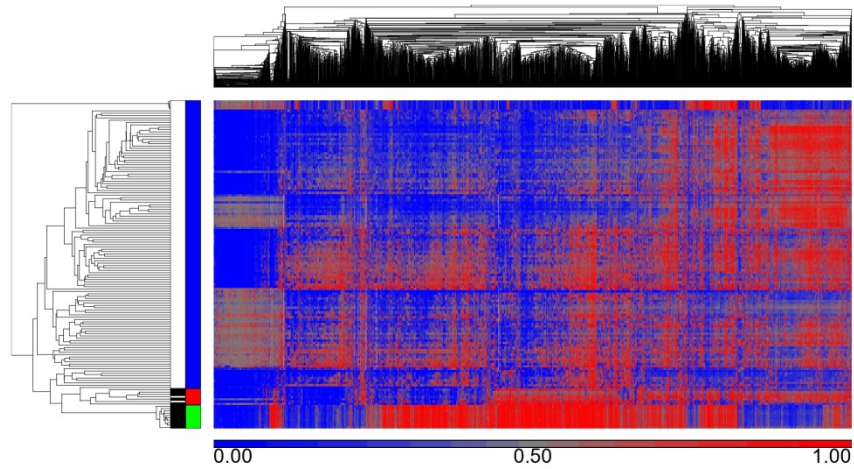


Fig.S10

A

Glioblastoma (WHO Grade IV)



B

WHO Grade II/III Glioma

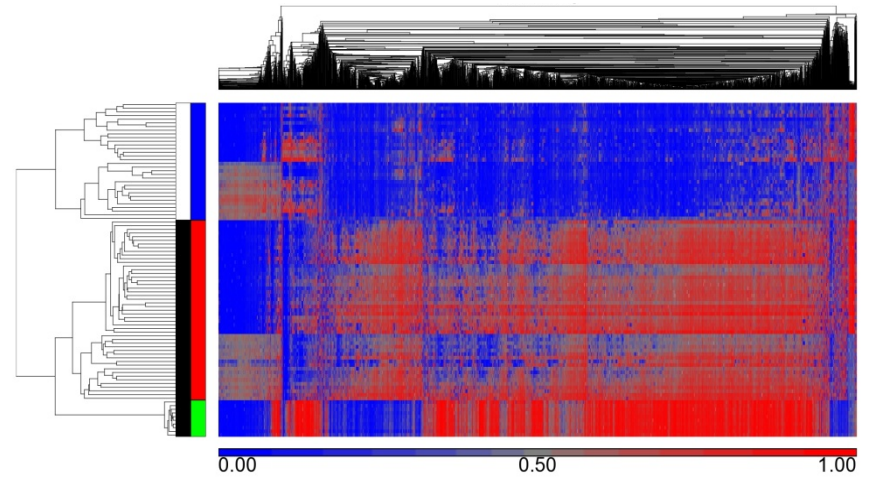
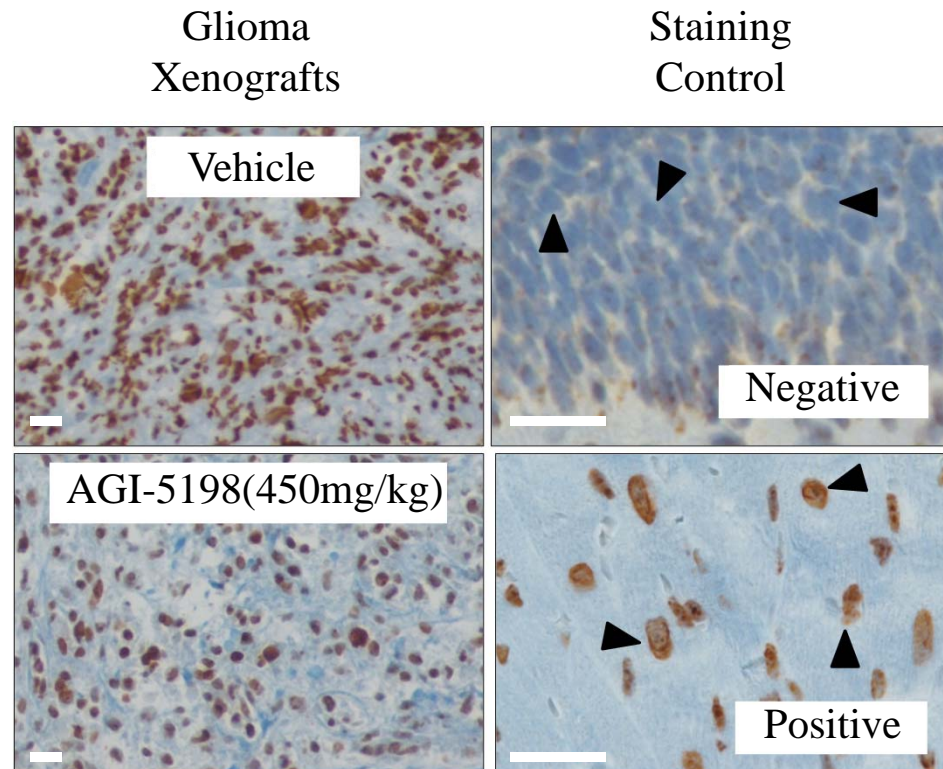


Fig.S11

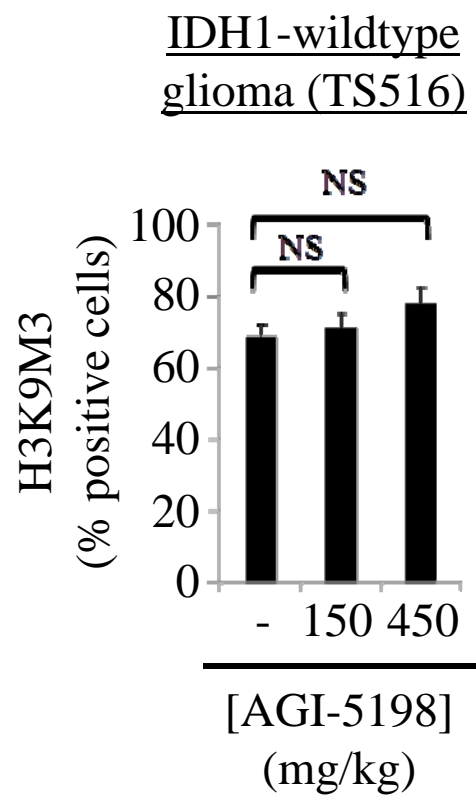
R132H-IDH1
(TS603 glioma)



IHC: H3K9m3

Fig.S12

A



B

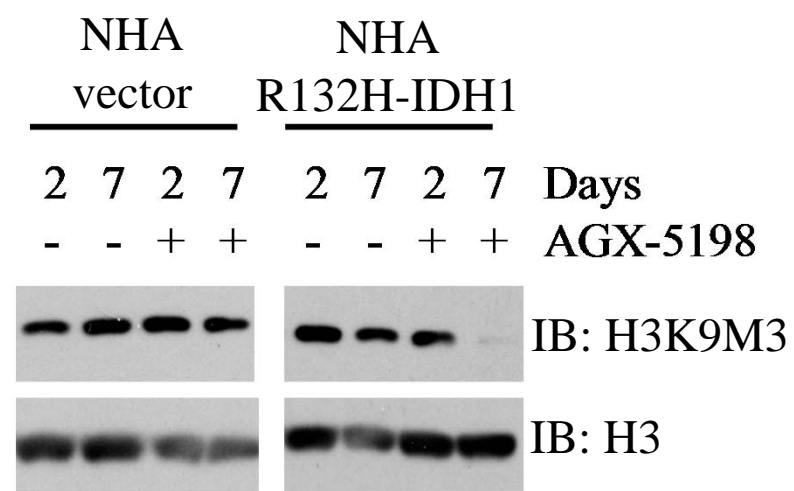


Fig.S13

R132H-IDH1
(TS603 glioma)

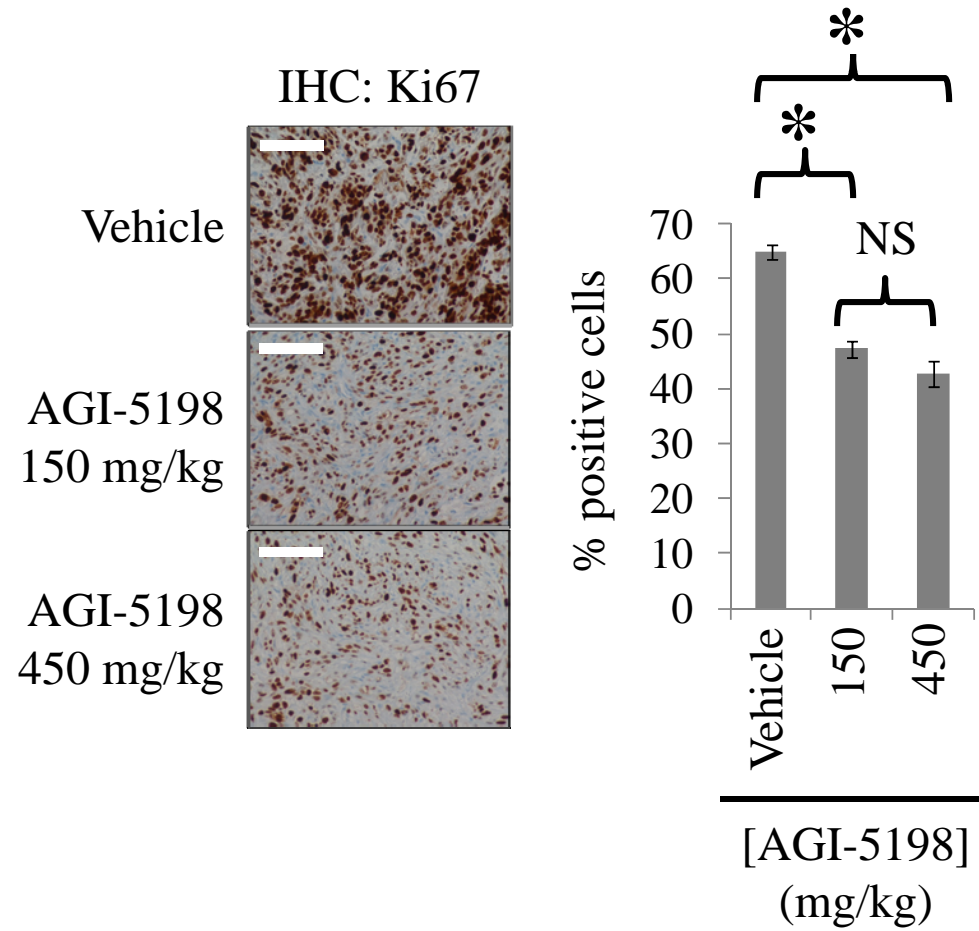


Fig.S14

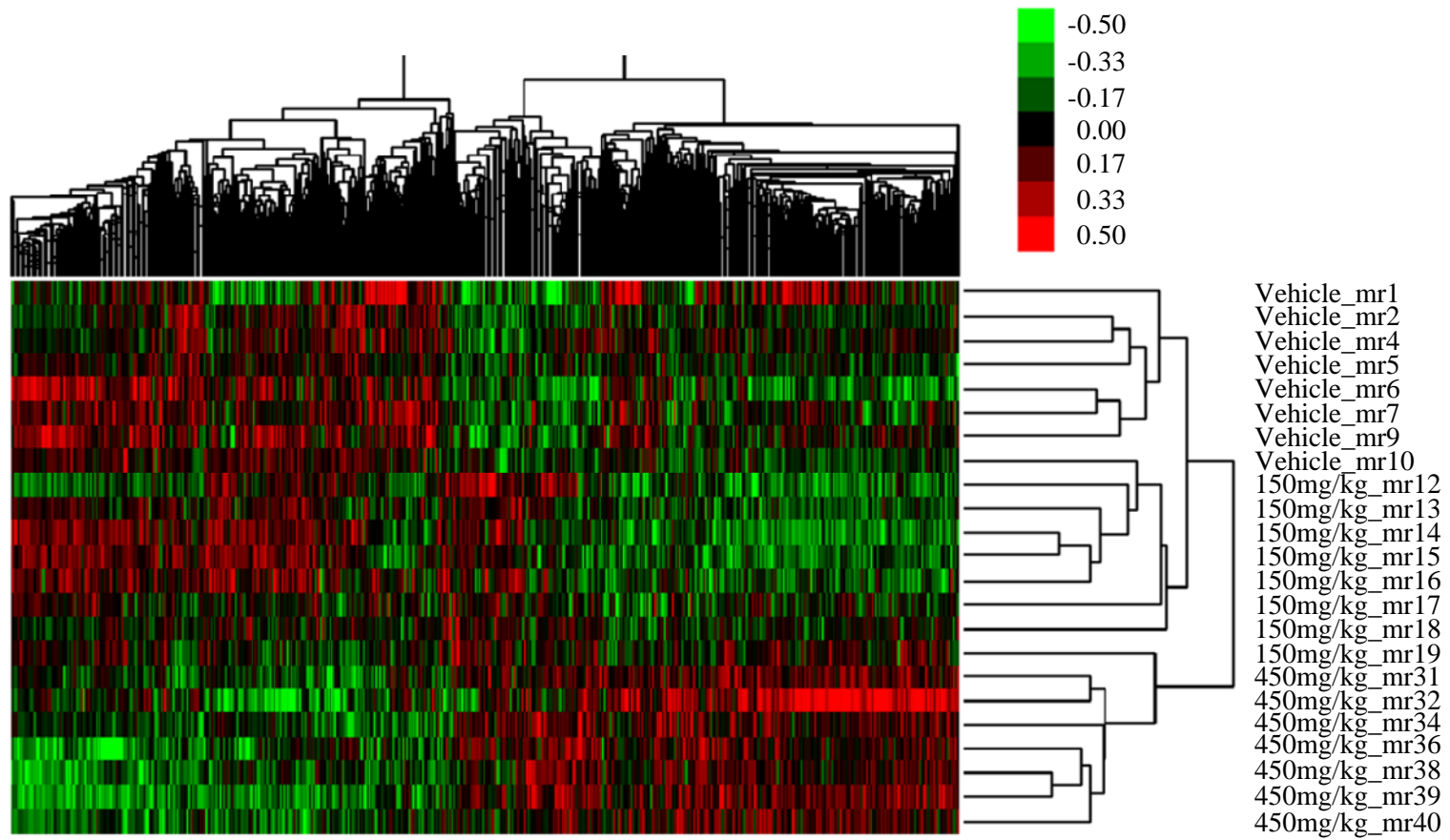


Fig.S15

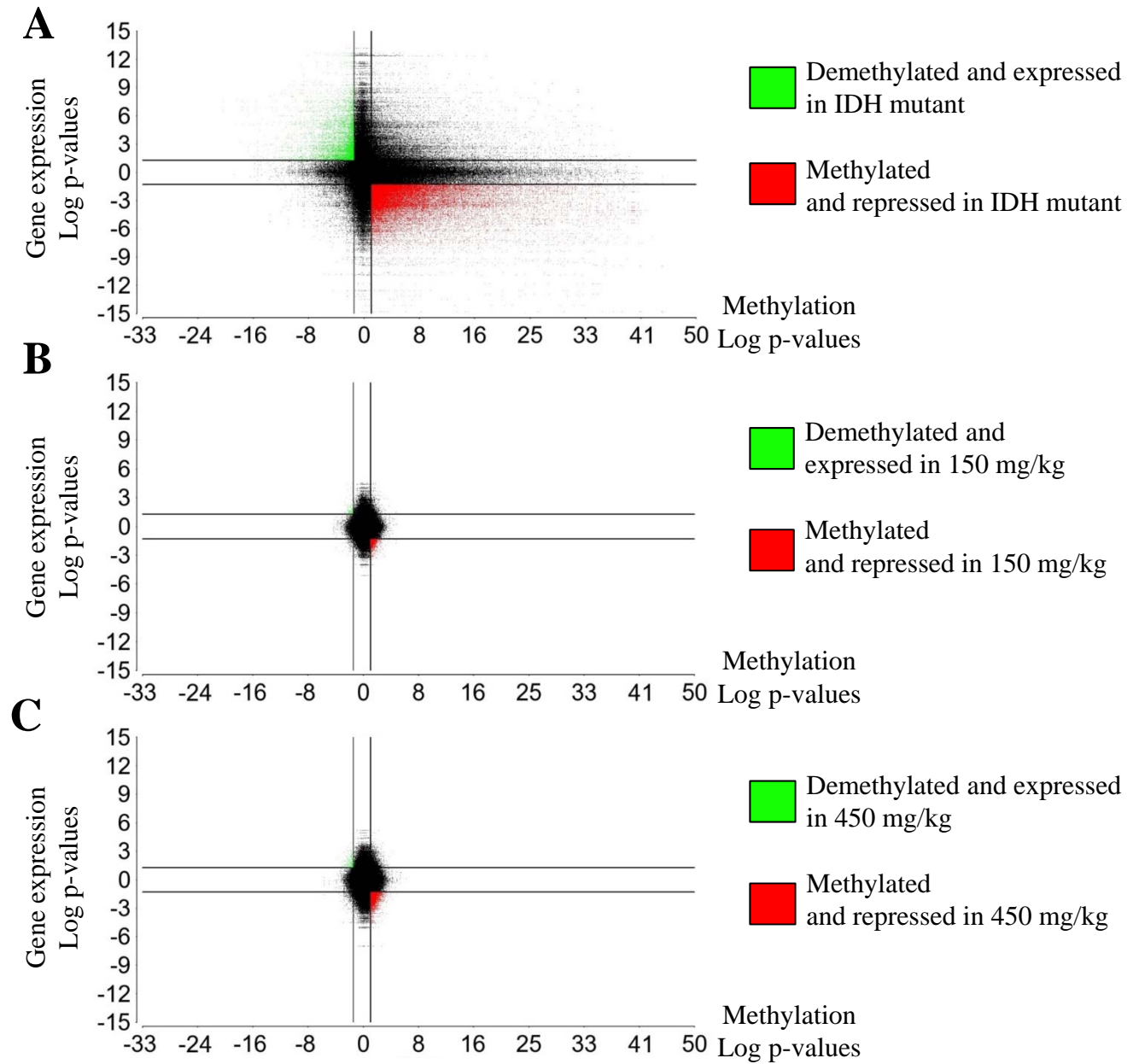


Fig.S16

